Photosynth Res (2006) 90:161–172
DOI 10.1007/s11120-006-9119-z

ORIGINAL PAPER

A method for quantitative analysis of spatially variable physiological processes across leaf surfaces

Mihai Aldea · Thomas D. Frank · Evan H. DeLucia

Received: 22 August 2006 / Accepted: 29 November 2006 / Published online: 9 January 2007

Abstract Many physiological processes are spatially variable across leaf surfaces. While maps of photosynthesis, stomatal conductance, gene expression, water transport, and the production of reactive oxygen species (ROS) for individual leaves are readily obtained, analytical methods for quantifying spatial heterogeneity and combining information gathered from the same leaf but with different instruments are not widely used. We present a novel application of tools from the field of geographical imaging to the multivariate analysis of physiological images. Procedures for registration and resampling, cluster analysis, and classification provide a general framework for the analysis of spatially resolved physiological data. Two experiments were conducted to illustrate the utility of this approach. Quantitative analysis of images of chlorophyll fluorescence and the production of ROS following simultaneous exposure of soybean leaves to atmospheric O_3 and soybean mosaic virus revealed that areas of the leaf where the operating quantum efficiency of PSII was depressed also experienced an accumulation of ROS. This correlation suggests a causal relationship between oxidative stress and inhibition of photosynthesis. Overlaying maps of leaf surface temperature and chlorophyll fluorescence following a photoinhibition treatment indicated that areas with low operating quantum efficiency of PSII also experienced reduced stomatal conductance (high temperature). While each of these experiments explored the covariance of two processes by overlaying independent images gathered with different instruments, the same procedures can be used to analyze the covariance of information from multiple images. The application of tools from geographic image analysis to physiological processes occurring over small spatial scales will help reveal the mechanisms generating spatial variation across leaves.

Keywords Chlorophyll fluorescence imaging · Quantitative image analysis · Reactive oxygen species · Spatial heterogeneity · Thermal imaging

M. Aldea
Program in Ecology and Evolutionary Biology, University of Illinois at Urbana-Champaign, Urbana, IL 61801, USA

T. D. Frank
Department of Geography, University of Illinois at Urbana-Champaign, Urbana, IL 61801, USA

E. H. DeLucia (✉)
Department of Plant Biology, University of Illinois at Urbana-Champaign, 265 Morrill Hall (MC 116), 505 S. Goodwin Ave, Urbana, IL 61801, USA
e-mail: delucia@life.uiuc.edu

Introduction

Geographical imaging methods developed for the analysis of satellite and other remote-sensing imagery hold great promise for advancing our understanding of plant physiological processes. These methods are tailored for the assembly and quantitative analysis of multiple images (layers) of the same landscape, acquired by one or more imaging platforms in different wavelengths of the electromagnetic spectrum. Inferences about ground cover are made by examining the statistical relationships among the spectral properties of different data layers (Frank 1988). Similarly, plant physiologists have the ability to examine multiple

Table 1 Examples of physiological processes that can be monitored remotely in vivo with digital imaging instruments to provide spatially resolved data

Parameter		Physiological process	Wavelength	References
Photosynthesis (kinetic measurements)	F_v/F_m	Maximum quantum efficiency of PSII	470/700	Genty et al. 1989; Rolfe and Scholes 1995; Oxborough 2004
	NPQ	Non-photochemical energy dissipation	470/700	
	Φ_{PSII}	Quantum yield of electron transport	470/700	
	Thermal	Transpiration, conductance	None/>1200	Jones 1999; Omasa and Takayama 2003
Water and energy status	MRI	Water transport	X-ray to microwaves	Gussoni et al. 2001; Clearwater and Clark 2003
	Tracers	Water transport	Depends on tracer	Gaff and O-Ogola 1971; Canny 1990
Leaf pigments	PRI	Xanthophyll cycle	<700/531,570	Ehrlich et al. 1994; McVicar and Jupp 1998; Gamon and Surfus 1999
	NDVI	Chlorophyll content	704,750/ 750,704	
Gene expression	GFP	Gene expression	485/509	Chalfie et al. 1994; Haseloff and Amos 1995; Dixit et al. 2006
	RFP	Gene expression	490,520,563/ 583	
	BFP	Gene expression	UV/440	
Defense compounds	Dyes	ROS (H_2O_2, radicals)	Visible light	Fryer et al. 2002

''Wavelength'' indicates typical excitation/measurement wavelength (nm). [MRI = magnetic resonance imaging; PRI = photochemical reflectance index; NDVI = normalized difference vegetation index; GFP, BFP, RFP = green, blue, and, respectively, red florescent protein]

spatially-resolved physiological processes (Table 1) occurring in the same leaf. For example, images of stomatal conductance, non-photochemical quenching, and Photosystem II operating efficiency can be acquired simultaneously using chlorophyll fluorescence and thermal imaging (Omasa and Takayama 2003; Aldea et al. 2006; Tang et al. 2006), while the spatial patterns of reactive oxygen species (ROS) can be mapped using specific dyes (Fryer et al. 2002). Quantitative comparisons among layers are rare and may reveal functional relationships between these processes. Because the data and analytical approaches used in plant physiology are similar to those used in remote sensing of landscapes, the methods used in geographical imaging (Swain and Davis 1978; Jensen 2005) are well suited to the analysis of spatial maps of physiological processes.

Photosynthesis and its component processes can be highly variable across the surfaces of individual leaves (Mott and Buckley 1998; Peak et al. 2004; West et al. 2005). Development (Grassi and Magnani 2005), variation in microenvironment (Peak et al. 2004), and stomatal conductance (Haefner et al. 1997; Prytz et al. 2003; West et al. 2005), as well as insect, pathogen or mechanical damage (Bown et al. 2002; Zangerl et al. 2002; Hall et al. 2004; Aldea et al. 2005; Gog et al. 2005) generated spatial heterogeneity of photosynthesis.

Understanding the mechanisms contributing to the spatial heterogeneity of photosynthesis has been hampered by an inability to precisely map and compare multiple physiological processes across leaf surfaces. It is now possible to quantify the spatial patterns of several different processes that may contribute to variation in photosynthesis, including the energy state of thylakoid membranes, the rate of electron transport through the photosystems, stomatal conductance, deployment of chemical defenses, gene expression, and water transport (Table 1). Although our ability to collect spatially resolved information for individual physiological processes is accelerating, simultaneous analysis of these different layers of information is uncommon. Studies of the spatial variation of photosynthesis typically employ analysis of single two-dimensional images (Nilsson 1980, 1995; Omasa and Takayama 2003; Smith et al. 2004). By quantifying the co-variance of information from multiple layers of data (Table 1) and using this new metadata set to identifying unique features, the use of quantitative image analysis will advance understanding of the mechanisms driving spatial variation in photosynthesis within individual leaves.

Different types of spatial variation in physiological processes across leaf surfaces require different analytical approaches. At one extreme is fine-grained

heterogeneity, characterized by many small, adjacent areas with different properties (high coefficient of variation). Variation in microenvironment (Eckstein et al. 1996; Mott and Buckley 2000; West et al. 2005), exposure to ozone (Morgan et al. 2004; Fiscus et al. 2005), localized changes in leaf hydraulic status (Mott and Franks 2001), and intrinsic variation in biochemical properties (Buckley et al. 2003) can generate fine-grained heterogeneity. At the other extreme is coarse-grained heterogeneity, characterized by large homogeneous areas with relatively well-defined edges (low coefficient of variation within a patch) followed by a step change to a new physiological state. Physical damage to leaves by insects often causes discrete areas of damage or coarse-grained heterogeneity of photosynthesis (Bown et al. 2002; Zangerl et al. 2002; Aldea et al. 2005, 2006; Tang et al. 2006).

The objective of this research was to apply the quantitative methods for image analysis developed for remote sensing (Swain and Davis 1978) to the spatial patterns of physiological processes across leaf surfaces. Two experiments were conducted to generate appropriate images. In the first experiment soybean plants were exposed simultaneously to elevated atmospheric ozone and soybean mosaic virus (SMV) to generate fine-grained heterogeneity in photosynthetic efficiency and related processes. In the second experiment a photoinhibition treatment to a discrete portion of a leaf was used to generate coarse-grained heterogeneity. For simplicity only two spatially resolved data sets (two layers) were collected in each experiment. In principle there is no limit to the number of data layers that can be combined with geographic image analysis techniques.

While specific methods will vary with the type of data and the objectives of the analysis, the following steps provide a general framework for the analysis of spatially-resolved physiological data: (1) registration and resampling, (2) cluster analysis, and (3) classification. *Registration and resampling* are used to precisely align and overlap images (spatial maps) of mechanistically related physiological processes (e.g., ROS and chlorophyll fluorescence). *Clustering* relies on multivariate statistics such as *cluster analysis* to identify groups of pixels with similar profiles (i.e., classes) and to quantify the covariance between maps of different physiological processes. A *classification* algorithm (i.e., Bayesian maximum likelihood) is then used to create a new spatial map of the combined metadata by assigning all the pixels in the image to one of the predefined classes. These steps allow the spatially—resolved analysis of statistical relationships between various leaf processes.

Methods

Fine-grained heterogeneity

To illustrate the analysis of fine-grain heterogeneity, the spatial pattern of the production of ROS and Photosystem II quantum operating efficiency (Φ_{PSII}) were measured on soybean leaves exposed to ozone and virus infection. Soybeans (*Glycine max* L., cv. Pioneer 93B15) were grown in 5-l pots in a growth chamber with a 14-h photoperiod (300 μmol m^{-2} s^{-1} PFD, 25°C), and an 8-h dark period (20°C) as in Aldea et al. (2005). Immediately after emergence, plants were fumigated with ozone (O_3) at ~80 nl l^{-1} for 8 h each day, centered within the photoperiod (ozone generator Model HTU-500AC, Azco Industries Ltd., Surrey, BC, Canada; O_3 analyzer Model 1008-RS, Dasibi Environmental Corp., Glendale, CA). The first fully expanded trifoliate was inoculated mechanically (Chen et al. 2004), homogenously across the leaf surface, with soybean mosaic virus (SMV).

The spatial pattern of Photosystem II operating efficiency (Φ_{PSII}) was quantified on attached leaves (first trifoliate) with an imaging chlorophyll fluorometer (Walz Imaging PAM, Walz GmbH, Effeltrich, Germany) ca. 100 h after infection with SMV. At a given incident irradiance and leaf absorptance, Φ_{PSII} is directly proportional to the rate of electron transport through the Photosystem II reaction centers (Genty et al. 1989; Rolfe and Scholes 1995). When other electron sinks are inhibited (e.g., photorespiration) or are insignificant (e.g., nitrate reduction) the rate of electron transport through PS II is proportional to the rate of carbon assimilation (Genty et al. 1989).

Leaves were measured under steady state, light-adapted conditions (229 μmol m^{-2} s^{-1} PFD; 23 × 33 mm imaged area). These irradiances were similar to the light environment of the growth chamber (average 300 μmol m^{-2} s^{-1}) and optimal for imaging chlorophyll fluorescence using the Walz Imaging PAM at its highest resolution. Each leaf was adapted to the new light environment for 5 min. The light-adapted steady-state fluorescence (F′) was then recorded with the measuring pulse from the fluorometer (Oxborough et al. 2000; Oxborough 2005). An image of the maximum fluorescence (F'_m) was recorded during a one-second saturating pulse (ca. 2,500 μmol m^{-2} s^{-1}). Photosystem II quantum operating efficiency (Φ_{PSII}) was calculated as the quotient $(F'_m–F')/F'_m$ (Genty et al. 1989).

Following chlorophyll fluorescence imaging, the leaves were harvested with a sharp razor blade while holding their petiole under degassed water. They were immediately vacuum-infiltrated with 10 mM nitroblue

tetrazolium (NBT; 0.2% Tween 80), placed in a water flask and returned to the growth chamber for 10 min. The light-yellow NBT reacts with superoxide and forms a dark-blue formazan precipitate (Fryer et al. 2002). Leaves were gently cleared of chlorophyll in cold dimethyl sulfoxide (DMSO) and washed with warm ethanol. The cleared leaves were photographed with a digital camera using diffuse backlight. After subtracting the non-formazan pixels (as in Fryer et al. 2002), the image was converted to grayscale and inverted (by subtracting all pixel values in the image from 255), such that the areas with most superoxide (darkest formazan deposits) became the brightest pixels (Image Invert, Photoshop 7.0.1, Adobe Systems Inc., San Jose, CA, USA).

Coarse-grained heterogeneity

To illustrate the analysis of coarse-grained heterogeneity, spatial variation in leaf temperature and chlorophyll fluorescence were measured on photoinhibited soybean leaves. Soybean plants were grown in growth chambers as described above but without ozone. Some plants were moved to a 4°C cold room (Gray et al. 2003) and the topmost fully-expanded trifoliate was covered with a layer of aluminum foil which had a window in the shape of a capital letter ''I''. After 1 h at low temperature a bright, cold light (ca. 2,500 μmol m^{-2} s^{-1} PFD) from a halogen microscope lamp illuminated the leaf for an additional 1 h. The aluminum foil was removed and plants were returned to the growth chamber for approximately 1 h before images were collected.

To quantify the spatial pattern of evapotranspiration leaf surface temperature was imaged with an infrared camera (ThermaCAM SC1000 Infrared Camera, FLIR Systems, Portland, OR, USA; wavelengths: 3–5 μm). We assumed that the variation in latent heat loss associated with evapotranspiration was the dominant process controlling heterogeneity in leaf surface temperature (Jones 1999; Omasa and Takayama 2003). The adaxial surface of an attached leaf was held perpendicular to the camera and in front of a warmer background to improve contrast (ca. 30°C; 150–200 mm behind the leaf). The thermal camera was calibrated for air temperature and humidity and leaf emissivity was assumed to be 1. Temperature differences on the same image were precise to ±0.07°C (instrument specifications).

The spatial patterns of PSII operating efficiency (Φ_{PSII}), ROS and leaf surface temperature were quantified using the remote sensing image analysis methods described by Swain and Davis (1978), implemented in a readily available geographical imaging software package (Erdas Imagine 8.6, Leica Geosystems GIS & Mapping LLC, Atlanta, GA, USA). These image analysis methods (Swain and Davis 1978) are available in most geographic image analysis or remote sensing software packages. Because of the similarity of the data and analysis needs, we were able to adapt these widely used image analysis tools from the field of remote sensing to the analysis of images representing physiological processes.

Understanding image data

The quantitative analysis of spatial maps of physiological processes (i.e., images) is based on the assumption that pixel intensity values can be related to a physiological process. Most commercially available chlorophyll fluorescence imaging instruments (e.g., Imaging PAM, Walz GmbH, Effeltrich, Germany; FluorImager, Technologica Ltd., Colchester, UK; FluorCam, PSI, Brno, Czech Republic) produce images with pixel values between 0 and 255 (unsigned 8-bit), which can be translated into meaningful physiological data using a linear function. For example, a spatial map of Photosystem II quantum operating efficiency (Φ_{PSII}) has pixel intensity values between 0 and 255, but the physiological range of this parameter varies from a minimum value (MIN) to a maximum (MAX), which can generally be determined within the application used to obtain the image. The conversion from pixel intensity to true value is:

$$\Phi_{PSII} = \{\text{pixel value}\} \times \frac{\text{MAX} - \text{MIN}}{255} + \text{MIN} \qquad (1)$$

For final presentation of the data it may be desirable to express the true value using Eq. 1 rather than relative pixel intensity values. However, for the purposes of image analysis, maintaining the unsigned 8-bit format is recommended, as it ensures comparable variances among the layers of an image, which may otherwise be on very different scales (e.g., Φ_{PSII} and temperature).

Image registration and resampling

Images collected with different instruments generally have different pixel resolutions and sizes. For example, images of Φ_{PSII} acquired with the Walz Imaging PAM are 640 by 480 pixels (307,200 pixels total); the camera was held at a fixed distance and captures 23 by 33 mm of the leaf surface (all pixels were square). This translates to a pixel size of approximately 50 μm or 1–5

plant cells per pixel. Thermal images (ThermaCAM SC1000, FLIR Systems, Portland, OR) were 255 by 239 pixels, but the size of leaf surface captured depends on the distance from the handheld camera to the leaf. The thermal images we collected had pixel sizes ranging from 100 μm to 600 μm. Images of ROS distribution also were collected with a handheld digital camera, resulting in pixel sizes from 20 μm to 150 μm, depending on the distance from the camera to the leaf. These discrepancies in resolution and pixel size between images acquired with different instruments or at different distances between the instruments and the leaf can be resolved using a technique that interchanges different spatial resolutions known as *resampling*. In our case, one of the images also required spatial adjustments for accurate alignment with the other images of the same leaf, a process called *registration*. Image resampling (or interpolation) is often guided by a registration solution, such that the resampled image will not only match the pixel resolution and size of the standard, but it will also be in perfect alignment with it. For accurate analyses, resampling must be performed using algorithms that preserve the underlying data in an image (i.e., pixel intensity).

Images of the same leaf (e.g., Φ_{PSII}, leaf surface temperature, ROS) were subjected to a first-degree polynomial transformation. This registration technique guided the rotation, translation, and linear stretch of the smaller image (i.e., fewer pixels) such that it accurately overlapped the larger image. The polynomial solution was computed based on 8–15 reference features visible in both images (e.g., intersections of major veins, necrotic spots, small holes), which were manually located in both images (Fig. 1a and b). It is possible, though considerably more difficult to register non-flat or wrinkled leaf surfaces by constructing flat projections using high-degree polynomial or trigonometric functions. The accuracy of registration is best examined visually (Fig. 1c) by checking the image overlap around edges or obvious surface structures such as veins. Some software packages (e.g., Erdas

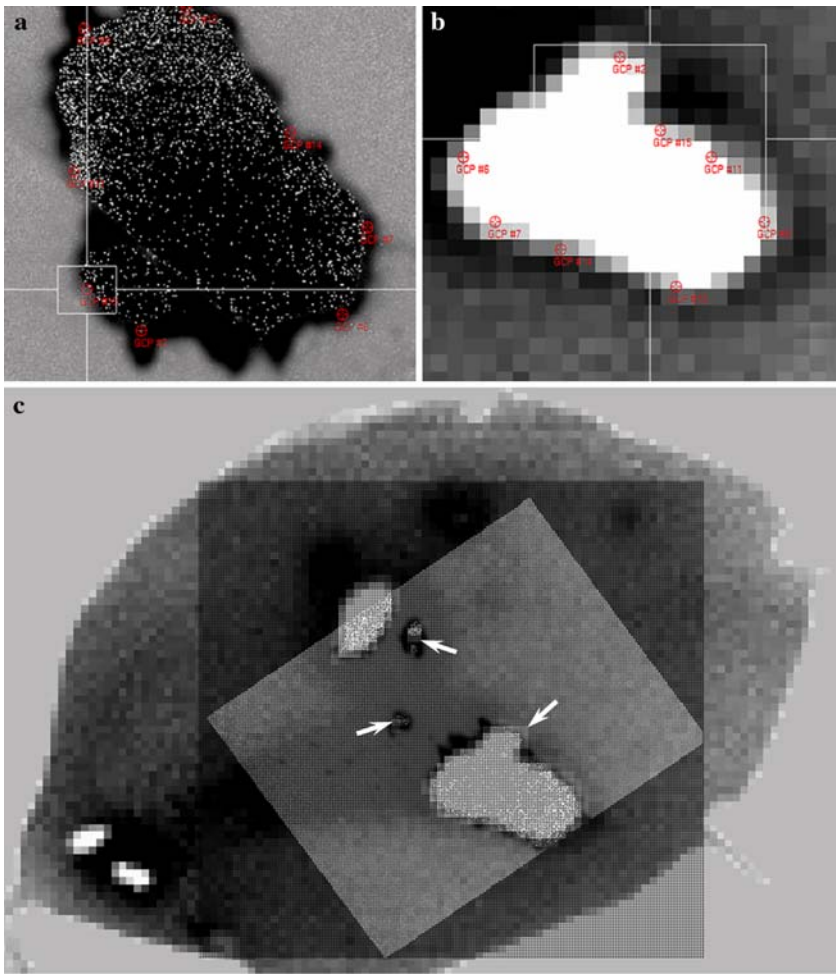

Fig. 1 Graphic representation of the registration process of two images with different resolutions acquired with different instruments. (**a**) Detail of an image of the Photosystem II quantum operating efficiency (Φ_{PSII}) of a soybean leaf with caterpillar damage; (**b**) detail of a thermal image of the same area of the leaf as shown in (a). Both images contain red registration points that were manually placed in corresponding areas on the two images (points with the same number should coincide); these reference points were used to register the two images with respect to each other. (**c**) After registration, the Φ_{PSII} image was overlapped (semitransparent for illustration purposes only) on top of the thermal image in a virtual image stack. Miss-aligned pixels (registration errors) are indicated by the white arrows

Imagine) also provide statistical measures of the accuracy of the registration by calculating residuals, RMS errors, and a match score for each registration reference point.

To prevent artifacts originating from pixel averaging, the smaller image always was registered with respect to the larger, such that all registered images were larger than the original. The original images were resampled using a nearest neighbor algorithm based on the polynomial solution to the registration. Nearest neighbor interpolation is the simplest method of image resampling, which simply changes pixel size and does not alter the underlying data (Swain and Davis 1978). The intensity of a pixel in the new image is the intensity of the nearest pixel of the original image. For example, if an image is enlarged by 200%, one pixel will become a 2 by 2 area of 4 pixels with the same intensity as the original pixel. Most software uses this type of interpolation to enlarge a digital image because it does not change the data in the image and does not introduce anti-aliasing errors (i.e., averaging of pixels around edges). Other resampling techniques include bilinear and bicubic convolution, where the pixel intensity in the new image is calculated using linear or cubic functions of the neighboring pixels in the original (Swain and Davis 1978). These later resampling methods produce a smoother appearance but may introduce artifacts in the resampled image, evident as halos or blurring near the edges of features and generally constitute unwanted deviations from the original data.

Following registration and resampling, images of the same leaf were overlaid as layers of a virtual image stack (Figs. 2c and 3c). Virtual image stacks can be thought of as three-dimensional matrices, where each pixel has a physical location in 2-D space (matrix) and a vertical set of spectral characteristics (i.e., intensity in each layer). Analyzing such data entails the identification of spatial patterns based on pixel values in all layers of the image stack. The only limit to the number of layers in an image is the amount of physical memory on the computer. To simplify the description of this method, only two layers were used for each analysis described below.

Clustering algorithms and feature-space diagrams

The objective of analyzing multi-layer images is to define discrete classes of pixels by minimizing in-class variance and maximizing the differences between classes; this multivariate statistical process is known as *clustering*. The relationships of the data in different layers of the image are then statistically examined within and between the classes, thus uncovering underlying trends in the data. Depending on the type of heterogeneity on each image, an automated or manual identification of the spectral variation can be performed to isolate classes of pixels based on their set of intensity values in all layers of the image (Swain and Davis 1978). Features can be identified manually (Fig. 2) by selecting areas of interest and allowing the software package to assemble their characteristics (mean, variance) into a class, or features can be identified automatically with an iterative self-organizing clustering algorithm (Fig. 3; ISODATA, Erdas Imagine 8.6, Leica Geosystems GIS & Mapping LLC, Atlanta, GA, USA; Swain and Davis 1978). Within each class it was possible to examine the covariance of the data from the overlaid layers, thus allowing a statistical understanding of spatial patterns of various processes mapped with different techniques and instruments.

Whether pixel classes are defined manually or automatically using clustering algorithms, their interpretation is based on the analyst's understanding of the images being classified or the objects in the image. The user must create enough classes to allow for all possible types of area on the image. Since classes can be merged but not split after they are created, generally it is better to initially classify the image into more classes than necessary. When classification algorithms are performed on satellite imagery, the meaning of each class is defined after ''ground-proofing'', which entails inspecting the ground area corresponding to each pixel class. Thus one or more pixel classes may be labeled as forest ecosystem, cornfield, or parking lot. Similarly, pixel classes isolated on spatial maps of physiological processes across leaf surfaces are assigned meaning or labels based on the area they correspond to on the original images and the analyst's understanding of the leaf processes generating the underlying data. Thus pixel classes on images of leaves may represent fungal infections, holes, veins, areas of depressed photosynthesis, or closed stomata.

To investigate the relationships between the data in each layer of an image stack, pixel intensities in all layers can be plotted against each other in two-dimensional plots known as *feature-space diagrams* (Figs. 2e and 3d). Pixel clusters can be plotted as standard deviation ellipses around means in feature-space diagrams, thus providing a visual representation of the statistical analyses. The covariance between the data layers can be examined within and between the classes, thus affording insights into possible functional relationships between the physiological processes mapped in the layers of the image stack.

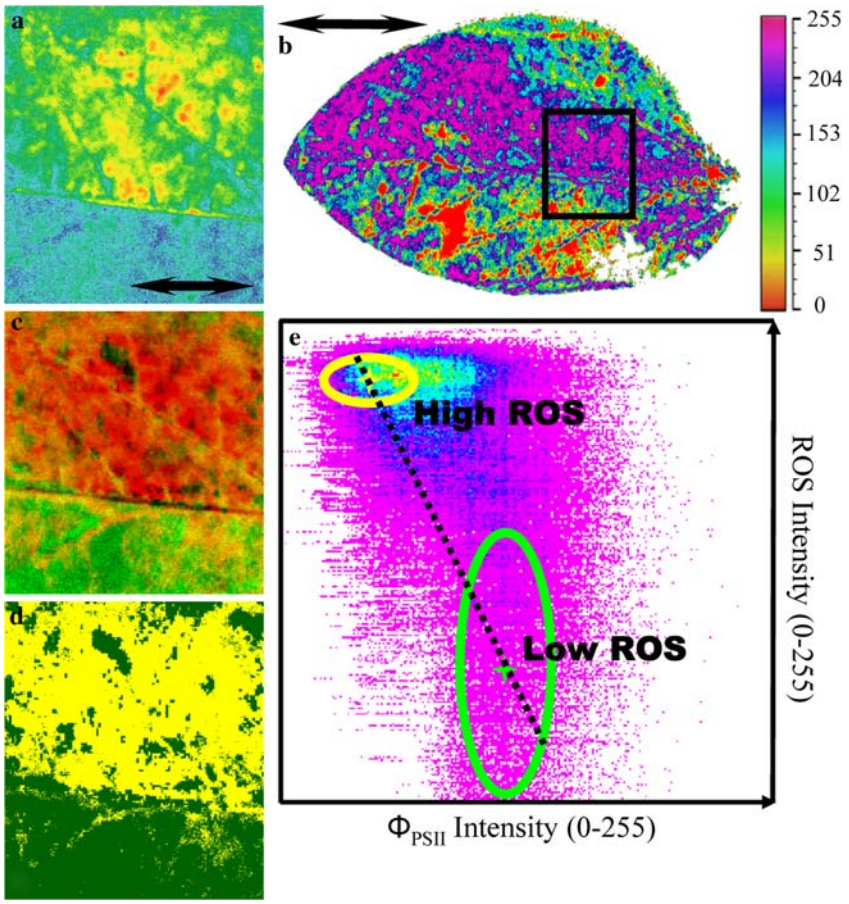

Fig. 2 The spatial patterns of Photosystem II quantum operating efficiency (Φ_{PSII}) and ROS, and a map image derived from quantitative image analysis for a soybean leaf exposed to ozone and SMV infection. (**a**) False color image of Φ_{PSII} (false color scale for variation in pixel intensity is illustrated to the right). Values for Φ_{PSII} were from 0.38 to 0.68; (**b**) False color image of ROS distribution (false color scale to the right, bar = 40 mm); (**c**) RG rendering of a two-layer image: Φ_{PSII} layer (green band) was stacked over the ROS map (red band) after registration. Combinations of red and green appear as yellow and orange; (**d**) An image map derived by a Bayes maximum likelihood algorithm that classified all pixels of the image (c) into two classes based on their intensity in the overlaid Φ_{PSII} and ROS layers. Green regions of the map represent areas with low ROS and high PSII efficiency values, while the yellow areas had high ROS and lower Φ_{PSII}. Images (a), (c), and (d) are on the same spatial scale and the bar in (a) represents 10 mm. (**e**) A feature-space diagram plotting the intensities of all pixels (8-bit) in the image stack (c). Φ_{PSII} pixel intensity is plotted on the *x*-axis and ROS on the *y*-axis. Ellipses (1-SD) around means (stars) for the two clusters were overlaid on this plot to evaluate the spectral properties of each class and their relationship to each other. This type of analysis quantitatively shows that pixels with high ROS values have lower Φ_{PSII} than areas with low ROS intensity. The color scale of feature-space plots represents the density of pixels plotted in a particular location; the gradient from no pixels to most pixels is illustrated by the color continuum: black, purple, blue, cyan, yellow, and orange

Classification algorithms and the map image

Spatial relationships between pixel classes can be examined by plotting their location using *supervised classification* algorithms (e.g., minimum distance, maximum likelihood; Swain and Davis 1978). For the types of images used in plant physiology (Table 1), Bayes maximum likelihood classification algorithms (Swain and Davis 1978) are best suited (though computationally intensive) to assign all the pixels in the image stack into the pixel classes formed by clustering algorithms. The location of the pixel classes can thus be spatially mapped by assigning each pixel in the image to a class using Bayes maximum likelihood decision rules (Swain and Davis 1978). The result of this type of analysis is a statistical representation of the spatial patterns observed in an image, as well as the relationships between the data contained in all layers. To investigate the accuracy of this type of classification, it is possible to create maps of the probability for each pixel to be assigned in its class. As with all Bayesian statistics a priori probabilities (default = 1 for all classes) can be used to reduce classification errors in areas where multiple classes overlap, and where pixels

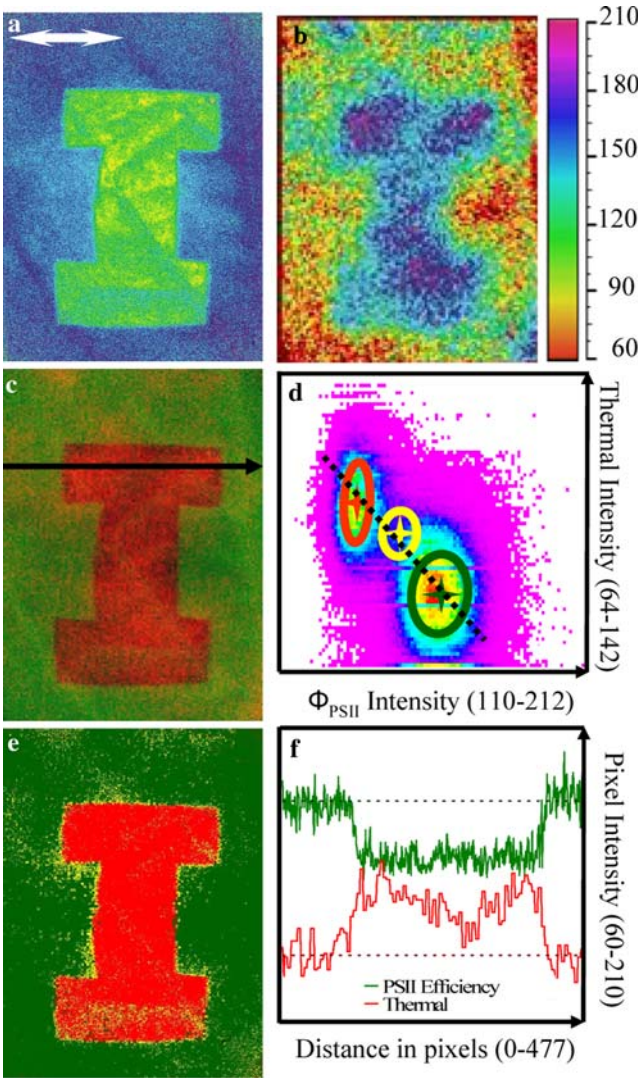

Fig. 3 The spatial patterns of Photosystem II quantum operating efficiency (Φ_{PSII}) and leaf surface temperature, and a map image derived from quantitative image analysis for a soybean leaf exposed to bright light at 4°C. (**a**) False color image of Φ_{PSII} (false color scale for variation in pixel intensity is illustrated to the right). Values for Φ_{PSII} were from 0.39 to 0.76; (**b**) False color image of leaf surface temperature. Temperature was from 24°C to 29°C; (**c**) RG rendering of a two-layer image: thermal layer (red band) was stacked over Φ_{PSII} layer (green band) after registration. Combinations of red and green appear as yellow and orange; (**d**) A feature-space diagram plotting the intensities of all pixels in the image stack (c). Φ_{PSII} pixel intensity is plotted on the *x*-axis and thermal on the *y*-axis. Ellipses (1-SD) around means (stars) for the three clusters were overlaid on this plot to evaluate the spectral properties of each class and their relationship to each other. This analysis quantitatively shows that pixels with high thermal values have lower Φ_{PSII} than those with lower thermal intensity. The color scale of feature-space plots represents the density of pixels plotted in a particular location; the gradient from no pixels to most pixels is illustrated by the color continuum: black, purple, blue, cyan, yellow, and orange. (**e**) Based on the signatures created by a clustering algorithm (ISODATA), a Bayes maximum likelihood classification placed all pixels of the image (c) into one of three classes. Green regions of the map represent areas with low temperature and high PSII efficiency values, while the red areas had high temperature and lower Φ_{PSII}. Transition areas with intermediate values in both the Φ_{PSII} and thermal layers are rendered in yellow; (**f**) A plot of pixel intensities along the arrow in (c) for the Φ_{PSII} and thermal bands. This type of plot illustrates the sharp transition from undamaged to damaged tissue in each layer as well as the relationship between the Φ_{PSII} and thermal data for the 1-pixel wide line along the arrow. Dotted reference lines indicate mean pixel intensity in each layer for the healthy areas of the leaf. Images (a), (b), (c), and (e) are on the same spatial scale and the bar in (a) represents 10 mm

may be more likely to belong in a different class than the one to which they were initially assigned.

Results and discussion

Analysis of fine-grained heterogeneity

Damage caused by exposure to ozone or viral infection tends to produce fine-grained spatial heterogeneity where small damaged areas are interspersed in healthy tissue. The potential contribution of high levels of ROS to reductions in photosynthesis following simultaneous exposure to O_3 and SMV was examined by overlaying images of ROS and Photosystem II quantum operating efficiency (Φ_{PSII}; Fig. 2). Because of the low within-patch covariance between the data in the image layers and large between-patch differences, the results of automated clustering were not biologically meaningful. Therefore, biologically significant initiation points were manually selected: three areas with low Φ_{PSII} (~2,400 pixels) were defined as one class of pixels, while three with high Φ_{PSII} (~2,400 pixels) constituted another class. Upon examining these two classes in feature-space it was evident that pixels with low Φ_{PSII} also had high ROS intensity, while pixels with higher Φ_{PSII} had lower intensity in the ROS layer (Fig. 2e). Based on these manually defined classes, a Bayes maximum likelihood classification mapped all the pixels in the image stack into two discreet areas, using the pixel intensity values in the Φ_{PSII} and ROS layers (Fig. 2d). Instead of analyzing the data pixel by pixel, we examined the relationship between the two classes in the entire data set (Fig. 2e), one class with low Φ_{PSII} (mean ± SD, 59 ± 17 pixel intensity units, 8-bit scale) and high ROS concentration (206 ± 28) and another class with higher Φ_{PSII} (120 ± 20) and lower ROS (86 ± 51). A strong negative correlation was observed between PSII operating efficiency and the concentration of superoxide radicals within this soybean leaf (dotted line, Fig. 2e). As expected, the two different

classes (green and yellow, Fig. 2e) did not have significant internal correlation between ROS concentration and Φ_{PSII} (Pearson $R < 0.01$) and occupied similar areas (High ROS area = 86×10^3 pixels; Low ROS area = 76×10^3 pixels). Also, when the intensities of *all pixels* in the two-layer image were plotted in feature-space (disregarding the two classes), Φ_{PSII} and ROS were negatively correlated (Pearson $R = 0.34$; $n = 195{,}349$; Fig. 2e). These statistical relationships may suggest that a threshold ROS concentration was required for a measurable decrease in Φ_{PSII}.

Whereas correlation does not automatically imply causality, using our understanding of oxidative stress mechanistic inferences can be made about the relationship between ROS concentration and depressions of Φ_{PSII} (Fryer et al. 2002, 2003; Ort and Baker 2002; Zou et al. 2005). Areas of the leaf affected by the virus responded with an oxidative burst (Heiser et al. 1998; Hernandez et al. 2004) and the damage caused by ROS to the cellular machinery may have depressed photosynthetic efficiency, as illustrated by the coincidence of high ROS and low Φ_{PSII} areas on the image, as well as the overall negative trend of their respective relationship.

Analysis of coarse-grained heterogeneity

Damage by fungal pathogens or by herbivorous insects often causes coarse-grained heterogeneity characterized by large contiguous patches of lower photosynthesis. This type of damage requires a different analytical approach from the analysis of fine-scaled heterogeneity. For the purposes of illustration, discrete patches of low photosynthesis (i.e., coarse-grained heterogeneity) were generated by exposing a defined area of a leaf to a photoinhibition treatment of bright light and chilling similar to Gray et al. (2003). Photodamage to PSII reaction centers and stomatal closure may contribute to the observed reduction in Φ_{PSII} within areas exposed to light. To illustrate the relationship between stomatal conductance and the depression of Φ_{PSII} for leaves exposed to bright light at low temperature, we registered and overlapped spatial maps of Φ_{PSII} and leaf surface temperature. A sharp increase in photodamage from the areas that were kept in the dark during the chilling treatment to the areas exposed to the brightest light was observable as a state change in Φ_{PSII} and temperature (Fig. 3f). This knowledge about the cause and spatial pattern of heterogeneity suggested that it can be effectively characterized by an automated clustering algorithm into three classes of pixels representing unaffected areas of the leaf, areas that were strongly photoinhibited, and a relatively small transition zone. Similar patterns of heterogeneity may be caused in nature by physical or insect damage to leaves (e.g., Aldea et al. 2005; Tang et al. 2006). An automated clustering algorithm (ISODATA) isolated this type of heterogeneity into three classes, based on the variance of the data in the Φ_{PSII} and thermal layers. The classes were then spatially mapped using Bayes maximum likelihood statistics (as described above).

Insofar as leaf surface temperature (Fig. 3b) is proportional to evapotranspiration rates (Jones 1999; Omasa and Takayama 2003), the higher temperature of areas exposed to bright light during the cold treatment suggests stomatal closure. These areas of the leaf also had lower quantum efficiency of Photosystem II (Fig. 3d and f). Our analysis illustrates two large, discrete patches on the leaf surface, one area with high leaf temperature (closed stomata) and low Φ_{PSII} (area = $84{\cdot}10^3$ pixels) and another area with control values of operating efficiency and low leaf temperature (normal stomatal operation; area = 200×10^3 pixels). The transition between these two larger clusters occupied a small area (area = 19×10^3 pixels). Based on all pixels in the image ($n = 304{,}803$), Φ_{PSII} and surface temperature were negatively correlated ($R = -0.44$, $P < 0.01$). The negative correlation between Φ_{PSII} and surface temperature also was illustrated by the three classes generated by ISODATA clustering (Fig. 3d). The negative correlation between leaf temperature and presumably stomatal conductance with Φ_{PSII} as well as the image map generated from this relationship suggests that these processes were functionally related following the photoinhibition treatment.

Challenges and limitations

While providing a number of advantages, the application of geographical imaging methods to research in plant physiology is not without limitations. For example, images acquired with very different resolutions or images of non-flat leaves may prove difficult to register accurately, especially if not enough features are visible on both images for registration reference points. Problems with registration may be severe when analyzing fine-grained heterogeneity or around edges of an image, but these errors are quantifiable and most of the time correctable. Images taken at an angle to the surface (as opposed to perpendicular) or images of non-flat surfaces such as leaves severely infected by pathogens also may prove challenging to accurately overlap even with complex transformations.

The multivariate statistics used for analysis of multi-layered images have the same limitations and sources of error as their classical analogues (McGarigal et al. 2000). Cluster analysis is inefficient with highly correlated data, but a principal component transformation may be performed to resolve this issue. Also, classification algorithms (e.g., Bayesian maximum likelihood) work best when the pixel classes are clearly separated in multivariate space. Misclassified pixels can be identified (see Methods) and the errors (generally minor) corrected either manually or by adjusting the a priori probabilities of the Bayesian maximum likelihood algorithm.

Conclusions

To take advantage of the full potential of spatially-resolved data, we now have the ability to statistically investigate the relationships between physiological processes with accurate spatial resolution, thus facilitating mechanistic inferences (Aldea et al. 2006). Heterogeneity can thus be quantitatively investigated on the basis of mechanistic, spatial, and functional relationships between the many physiological processes that can be measured using imaging techniques (Table 1). The covariance of data in different maps of physiological processes overlaid in an image stack can be statistically examined by cluster analysis and graphically in feature-space diagrams. Finally, classification algorithms allow the creation of map images and thus the examination of spatial relationships among heterogeneity features on an image (e.g., area measurements, shape, spatial distribution).

Whereas the mechanisms of photoinhibition are fairly well understood (Gray et al. 2003), the link between ROS and depression of photosynthetic efficiency warrants further investigation. Using image analysis tools we observed a statistical relationship between the accumulation of ROS and reductions in photosynthetic efficiency (Φ_{PSII}) in leaves damaged simultaneously by O_3 and viral infection. There is increasing evidence that many types of damage—from mechanical, insect, and pathogen injuries to photoinhibition and cold stress—trigger a fast, potentially self-destructive oxidative burst in the affected tissues immediately following injury (Bi and Felton 1995; Thordal-Christensen et al. 1997; Leon et al. 2001; Bown et al. 2002; Gray et al. 2003; Hall et al. 2004; Zou et al. 2005). This type of stress response includes localized production of H_2O_2, superoxide radicals, and other ROS (Bi and Felton 1995; Thordal-Christensen et al. 1997; Repka 2002; Fryer et al. 2003) that impair physiological processes or kill cells (Wright et al. 2000; Chaerle et al. 2004). Using geographical imaging methods we overlapped spatial maps of Φ_{PSII} and ROS and examined the covariance of the data in the two spatially—resolved datasets. Areas with depressed PSII operating efficiency corresponded to areas of high ROS concentration (Fig. 2e) and there was a significant overall negative covariance between Φ_{PSII} and ROS. This offered quantitative, spatial, and statistical support for the hypothesis that stress-induced ROS may lead to depressed photosynthesis.

Acknowledgements We thank H. Bohnert for the use of the thermal camera, S. Clough and D. Bilgin for assistance with the virus inoculation, and S. Long and C. Chen for the use of the ozone generator. This research was supported by grants from the National Science Foundation (IBN 0326053) and USDA NRI (2002-02723). The authors do not specifically or implicitly endorse or promote the use of any of the equipment, products or software mentioned in the text.

References

Aldea M, Hamilton JG, Resti JP et al (2005) Indirect effects of insect herbivory on leaf gas exchange in soybean. Plant Cell Environ 28:402–411

Aldea M, Hamilton JG, Resti JP et al (2006) Comparison of photosynthetic damage from arthropod herbivory and pathogen infection in understory hardwood saplings. Oecologia 149:221–232

Bi JL, Felton GW (1995) Foliar oxidative stress and insect herbivory: primary compounds, secondary metabolites, and reactive oxygen species as components of induced resistance. J Chem Ecol 21:1511–1529

Bown AW, Hall DE, MacGregor KB (2002) Insect footsteps on leaves stimulate the accumulation of 4-aminobutyrate and can be visualized through increased chlorophyll fluorescence and superoxide production. Plant Physiol 129:1430–1434

Buckley TN, Mott KA, Farquhar GD (2003) A hydromechanical and biochemical model of stomatal conductance. Plant Cell Environ 26:1767–1785

Canny MJ (1990) Tansley review No. 22—what becomes of the transpiration stream? New Phytol 114:341–368

Chaerle L, Hagenbeek D, De Bruyne E et al (2004) Thermal and chlorophyll-fluorescence imaging distinguish plant–pathogen interactions at an early stage. Plant Cell Physiol 45:887–896

Chalfie M, Tu Y, Euskirchen G et al (1994) Green fluorescent protein as a marker for gene-expression. Science 263:802–805

Chen P, Buss GR, Tolin SA (2004) Reaction of soybean to single and double inoculation with different soybean mosaic virus strains. Crop Prot 23:965–971

Clearwater MJ, Clark CJ (2003) In vivo magnetic resonance imaging of xylem vessel contents in woody lianas. Plant Cell Environ 26:1205–1214

Dixit R, Cyr R, Gilroy S (2006) Using intrinsically fluorescent proteins for plant cell imaging. Plant J 45:599–615

Eckstein J, Beyschlag W, Mott KA et al (1996) Changes in photon flux can induce stomatal patchiness. Plant Cell Environ 19:1066–1074

Ehrlich D, Estes JE, Singh A (1994) Applications of NOAA-AVHRR 1 km data for environmental monitoring. Int J Remote Sens 15:145–161

Fiscus EL, Booker FL, Burkey KO (2005) Crop responses to ozone: uptake, modes of action, carbon assimilation and partitioning. Plant Cell Environ 28:997–1011

Frank TD (1988) Mapping dominant vegetation communities in the Colorado Rocky Mountain front range with Landsat Thematic Mapper and digital terrain data. Photogramm Eng Remote Sens 54:1727–1734

Fryer MJ, Ball L, Oxborough K et al (2003) Control of *Ascorbate Peroxidase 2* expression by hydrogen peroxide and leaf water status during excess light stress reveals a functional organisation of *Arabidopsis* leaves. Plant J 33:691–705

Fryer MJ, Oxborough K, Mullineaux PM et al (2002) Imaging of photo-oxidative stress responses in leaves. J Exp Bot 53:1249–1254

Gaff DF, O-Ogola O (1971) The use of nonpermeating pigments for testing the survival of cells. J Exp Bot 22:756–758

Gamon JA, Surfus JS (1999) Assessing leaf pigment content and activity with a reflectometer. New Phytol 143:105–117

Genty B, Briantais JM, Baker NR (1989) The relationship between the quantum yield of photosynthetic electron-transport and quenching of chlorophyll fluorescence. Biochim Biophys Acta 990:87–92

Gog L, Berenbaum MR, DeLucia EH et al (2005) Autotoxic effects of essential oils on photosynthesis in parsley, parsnip and rough lemon. Chemoecol 15:115–119

Grassi G, Magnani F (2005) Stomatal, mesophyll conductance and biochemical limitations to photosynthesis as affected by drought and leaf ontogeny in ash and oak trees. Plant Cell Environ 28:834–849

Gray GR, Hope BJ, Qin X et al (2003) The characterization of photoinhibition and recovery during cold acclimation in *Arabidopsis thaliana* using chlorophyll fluorescence imaging. Physiol Plantarum 119:365–375

Gussoni M, Greco F, Vezzoli A et al (2001) Magnetic resonance imaging of molecular transport in living morning glory stems. Magn Reson Imaging 19:1311–1322

Haefner JW, Buckley TN, Mott KA (1997) A spatially explicit model of patchy stomatal responses to humidity. Plant Cell Environ 20:1087–1097

Hall DE, MacGregor KB, Nijsse J et al (2004) Footsteps from insect larvae damage leaf surfaces and initiate rapid responses. Eur J Plant Pathol 110:441–447

Haseloff J, Amos B (1995) GFP in plants. Trends Genet 11:328–329

Heiser I, Osswald W, Elstner EF (1998) The formation of reactive oxygen species by fungal and bacterial phytotoxins. Plant Physiol Biochem 36:703–713

Hernandez JA, Rubio M, Olmos E et al (2004) Oxidative stress induced by long-term plum pox virus infection in peach (*Prunus persica*). Physiol Plant 122:486–495

Jensen JR (2005) Introductory digital image processing: a remote sensing perspective, 3rd edn. Upper Saddle River, NJ, Prentice Hall

Jones H (1999) Use of thermography for quantitative studies of spatial and temporal variation of stomatal conductance over leaf surfaces. Plant Cell Environ 22:1043–1055

Leon J, Rojo E, Sanchez-Serrano JJ (2001) Wound signaling in plants. J Exp Bot 52:1–9

McGarigal K, Cushman S, Stafford S (2000) Multivariate statistics for wildlife and ecology research. Springer-Verlag, New York, NY

McVicar TR, Jupp DLB (1998) The current and potential operational uses of remote sensing to aid decisions on drought exceptional circumstances in Australia: a review. Agric Syst 57:399–468

Morgan PB, Bernacchi CJ, Ort DR et al (2004) An in vivo analysis of the effect of season-long open-air elevation of ozone to anticipated 2050 levels on photosynthesis in soybean. Plant Physiol 135:2348–2357

Mott KA, Buckley TN (1998) Stomatal heterogeneity. J Exp Bot 49:407–417

Mott KA, Buckley TN (2000) Patchy stomatal conductance: emergent collective behaviour of stomata. Trends Plant Sci 5:258–262

Mott KA, Franks PJ (2001) The role of epidermal turgor in stomatal interactions following a local perturbation in humidity. Plant Cell Environ 24:657–662

Nilsson HE (1980) Remote sensing and image processing for disease assessment. Protection Ecol 2:271–274

Nilsson HE (1995) Remote-sensing and image-analysis in plant pathology. Annu Rev Phytopathol 33:489–527

Omasa K, Takayama K (2003) Simultaneous measurement of stomatal conductance, non-photochemical quenching, and photochemical yield of Photosystem II in intact leaves by thermal and chlorophyll fluorescence imaging. Plant Cell Physiol 44:1290–1300

Ort DR, Baker NR (2002) A photoprotective role for O_2 as an alternative electron sink in photosynthesis. Curr Opin Plant Biol 5:193–198

Oxborough K (2004) Imaging of chlorophyll a fluorescence: theoretical and practical aspects of an emerging technique for the monitoring of photosynthetic performance. J Exp Bot 55:1195–1205

Oxborough K (2005) Using chlorophyll a fluorescence imaging to monitor photosynthetic performance. In: Govindjee, Papageorgiou GC (eds) Chlorophyll fluorescence: a signature of photosynthesis. Kluwer Academic Press, Dordrecht, pp 409–428

Oxborough K, Hanlon ARM, Underwood GJC et al (2000) In vivo estimation of the Photosystem II photochemical efficiency of individual microphytobenthic cells using high-resolution imaging of chlorophyll a fluorescence. Limnol Oceanogr 45:1420–1425

Peak D, West JD, Messinger SM et al (2004) Evidence for complex, collective dynamics and emergent, distributed computation in plants. Proc Natl Acad Sci USA 101:918–922

Prytz G, Futsaether CM, Johnsson A (2003) Thermography studies of the spatial and temporal variability in stomatal conductance of *Avena* leaves during stable and oscillatory transpiration. New Phytol 158:249–258

Repka V (2002) Chlorophyll-deficient mutant in oak (*Quercus petraea* L.) displays an accelerated hypersensitive-like cell death and an enhanced resistance to powdery mildew disease. Photosynthetica 40:183–193

Rolfe SA, Scholes JD (1995) Quantitative imaging of chlorophyll fluorescence. New Phytol 131:69–79

Smith WK, Brodersen CR, Hancock TE et al (2004) Integrated plant temperature measurement using heat-sensitive paint and colour image analysis. Funct Ecol 18:148–153

Swain PH, Davis SM (eds) (1978) Remote sensing: the quantitative approach. McGraw-Hill International Book Co., New York, NY

Tang JY, Zielinski RE, Zangerl AR et al (2006) The differential effects of herbivory by first and fourth instars of *Trichoplusia ni* (Lepidoptera: Noctuidae) on photosynthesis in *Arabidopsis thaliana*. J Exp Bot 57:527–536

Thordal-Christensen H, Zhang Z, Wei Y et al (1997) Subcellular localization of H_2O_2 in plants. H_2O_2 accumulation in

papillae and hypersensitive response during the barley-powdery mildew interaction. Plant J 11:1187–1194

West JD, Peak D, Peterson JQ et al (2005) Dynamics of stomatal patches for a single surface of *Xanthium strumarium* L. leaves observed with fluorescence and thermal images. Plant Cell Environ 28:633–641

Wright KM, Duncan GH, Pradel KS et al (2000) Analysis of the *N*Gene hypersensitive response induced by a fluorescently tagged tobacco mosaic virus. Plant Physiol 123:1375–1385

Zangerl AR, Hamilton JG, Miller TJ et al (2002) Impact of folivory on photosynthesis is greater than the sum of its holes. Proc Natl Acad Sci USA 99:1088–1091

Zou JJ, Rodriguez-Zas S, Aldea M et al (2005) Expression profiling soybean response to *Pseudomonas syringae* reveals new defense-related genes and rapid HR-specific downregulation of photosynthesis. Mol Plant–Microbe Interact 18:1161–1174